RESEARCH BRIEF

Modulation of CD22 Protein Expression in Childhood Leukemia by Pervasive Splicing Aberrations: Implications for CD22-Directed Immunotherapies

Sisi Zheng[1,2], Elisabeth Gillespie[1], Ammar S. Naqvi[1,3], Katharina E. Hayer[1,3], Zhiwei Ang[1], Manuel Torres-Diz[1], Mathieu Quesnel-Vallières[4,5], David A. Hottman[2], Asen Bagashev[1,2], John Chukinas[2], Carolin Schmidt[1], Mukta Asnani[1], Rawan Shraim[1,3], Deanne M. Taylor[3], Susan R. Rheingold[2,6], Maureen M. O'Brien[7], Nathan Singh[8], Kristen W. Lynch[5], Marco Ruella[8], Yoseph Barash[4], Sarah K. Tasian[2,6], and Andrei Thomas-Tikhonenko[1,2,6,9]

ABSTRACT Downregulation of surface epitopes causes postimmunotherapy relapses in B-lymphoblastic leukemia (B-ALL). Here we demonstrate that mRNA encoding *CD22* undergoes aberrant splicing in B-ALL. We describe the plasma membrane–bound CD22 Δex5–6 splice isoform, which is resistant to chimeric antigen receptor (CAR) T cells targeting the third immunoglobulin-like domain of CD22. We also describe splice variants skipping the AUG-containing exon 2 and failing to produce any identifiable protein, thereby defining an event that is rate limiting for epitope presentation. Indeed, forcing exon 2 skipping with morpholino oligonucleotides reduced CD22 protein expression and conferred resistance to the CD22-directed antibody–drug conjugate inotuzumab ozogamicin *in vitro*. Furthermore, among inotuzumab-treated pediatric patients with B-ALL, we identified one nonresponder in whose leukemic blasts Δex2 isoforms comprised the majority of *CD22* transcripts. In a second patient, a sharp reduction in CD22 protein levels during relapse was driven entirely by increased *CD22* exon 2 skipping. Thus, dysregulated *CD22* splicing is a major mechanism of epitope downregulation and ensuing resistance to immunotherapy.

SIGNIFICANCE: The mechanism(s) underlying downregulation of surface CD22 following CD22-directed immunotherapy remains underexplored. Our biochemical and correlative studies demonstrate that in B-ALL, CD22 expression levels are controlled by inclusion/skipping of *CD22* exon 2. Thus, aberrant splicing of *CD22* is an important driver/biomarker of *de novo* and acquired resistance to CD22-directed immunotherapies.

See related commentary by Bourcier and Abdel-Wahab, p. 87.

[1]Division of Cancer Pathobiology, Children's Hospital of Philadelphia, Philadelphia, Pennsylvania. [2]Division of Oncology, Children's Hospital of Philadelphia, Philadelphia, Pennsylvania. [3]Department of Biomedical and Health Informatics, Children's Hospital of Philadelphia, Philadelphia, Pennsylvania. [4]Department of Genetics, Perelman School of Medicine at the University of Pennsylvania, Philadelphia, Pennsylvania. [5]Department of Biochemistry and Biophysics, Perelman School of Medicine at the University of Pennsylvania, Philadelphia, Pennsylvania. [6]Department of Pediatrics, Perelman School of Medicine at the University of Pennsylvania, Philadelphia, Pennsylvania. [7]Cincinnati Children's Hospital Medical Center, University of Cincinnati College of Medicine, Cincinnati, Ohio. [8]Department of Medicine, Perelman School of Medicine at the University of Pennsylvania, Philadelphia, Pennsylvania. [9]Department of Pathology and Laboratory Medicine, Perelman School of Medicine at the University of Pennsylvania, Philadelphia, Pennsylvania.

Note: Supplementary data for this article are available at Blood Cancer Discovery Online (https://bloodcancerdiscov.aacrjournals.org/).

S.K. Tasian and A. Thomas-Tikhonenko are co-senior authors of this article.

Current address for S. Zheng: Department of Pediatrics, UT Southwestern Medical Center, Dallas, Texas.

Corresponding Authors: Andrei Thomas-Tikhonenko, Children's Hospital of Philadelphia, 4056 Colket Translational Research Building, 3501 Civic Center Boulevard, Philadelphia, PA 19104-4399. Phone: 267-426-9699; E-mail: andreit@pennmedicine.upenn.edu; and Sarah K. Tasian, tasians@chop.edu

Blood Cancer Discov 2022;3:103–15

doi: 10.1158/2643-3230.BCD-21-0087

INTRODUCTION

Every year, children with high-risk B-lymphoblastic leukemia (B-ALL) account for a substantial number of pediatric cancer–related deaths. Outcomes for adults with B-ALL are even worse, with 5-year event-free survival less than 50% (1). A major breakthrough in the treatment of B-ALL has been the development of immunotherapeutics, particularly those directed against CD19. Examples include the CD19/CD3 bispecific T-cell engager blinatumomab, as well as tisagenlecleucel and axicabtagene ciloleucel, CD19-directed chimeric antigen receptor (CAR) T cells (2). Despite these successes, relapses occur in approximately 50% of B-ALL patients treated with CD19 CAR T cell immunotherapy by two broad mechanisms: (i) immune rejection and CAR T cell exhaustion usually leading to CD19-positive relapses and (ii) lymphoid-to-myeloid lineage switch or targeted epitope loss causing CD19-negative relapses (3–6). We and others previously reported that the emergence of surface CD19-negative relapses is driven by a combination of loss-of-function mutations, protein misfolding, and/or aberrant splicing (AS; refs. 7–11; reviewed in ref. 12). While several B-lineage markers, such as CD20 and CD79B, are considered to be promising targets (13, 14) in B-cell malignancies, CD22 has emerged as a prevalent and excellent alternative to CD19 for immunotherapeutic targeting in B-ALL relapse and increasingly in the first-line setting (15).

CD22 expression is restricted to B cells where it acts primarily to inhibit B-cell receptor (BCR)–mediated signaling through its immunoreceptor tyrosine-based inhibitory motifs (ITIM) in the cytoplasmic tail (16, 17). The canonical form of CD22 also acts as a highly glycosylated sialic acid–binding receptor composed of seven extracellular immunoglobulin-like (Ig-like) domains at its N-terminus. These N-terminal domains can be targeted with CD22-directed immunotherapies, including anti-CD22 CAR T cells (18) and the antibody–drug conjugate inotuzumab ozogamicin (19–22). These modalities have achieved remarkable success in inducing remissions in children and adults with chemotherapy-refractory B-ALL. Nonetheless, a significant fraction of patients relapse over time due to downmodulation of CD22 expression without complete protein loss.

Molecular mechanism(s) underlying this phenomenon remain poorly understood (23). The fact that CD22 protein downregulation after CD22-directed CAR T cell immunotherapy is not always commensurate with a decrease in *CD22* mRNA (18) suggests a possible posttranscriptional mechanism of protein loss, such as AS. In fact, *CD22* is known to undergo AS, and prior studies have suggested that the C-terminal truncation of CD22 may contribute to a more aggressive phenotype (24, 25). However, the role of CD22 splice isoforms in the context of immunotherapeutic response have not previously been characterized. Here, we report the identification of a novel *CD22* Δex5–6 isoform and several *CD22* Δex2* variants present at baseline in human B-ALL and investigate their potential involvement in *de novo* and acquired resistance to CD22-directed immunotherapies.

RESULTS

CD22 Transcript Is Aberrantly Spliced in B-ALL

To characterize comprehensively splicing variations within the *CD22* transcript that are prevalent in B-ALL, we obtained RNA sequencing (RNA-seq) data from a cohort of 219 pediatric B-ALL samples from the NCI Therapeutically Applicable Research to Generate Effective Treatments (TARGET) consortium (26) and compared them with the RNA-seq data of normal B-cell subpopulations derived from 11 healthy donors through the BLUEPRINT consortium (27) and the leukemia biorepository at the Children's Hospital of Philadelphia Center for Childhood Cancer Research (CHOP CCCR). By applying the previously developed Modeling Alternative Junction Inclusion Quantification (MAJIQ) algorithm (28), we quantified numerous local splicing variations (LSV) in pediatric B-ALL. *CD22* emerged as a highly aberrantly spliced transcript, with noncanonical isoforms involving nearly all exons, particularly those corresponding to the extracellular domain of the protein. Furthermore, among existing B-cell immunotherapeutic targets, *CD22* demonstrated the highest degree of splicing complexity as measured by the total number of LSVs within the gene, even when normalized by exon count (Fig. 1A; Supplementary Fig. S1). The splicing variations involved not only the previously studied 3′-terminal exon 12 (24, 25), but also exons 5 and 6 (Fig. 1B), which encode the third and fourth extracellular Ig-like domains of CD22 and therefore could affect responses to immunotherapy. We also identified five isoforms that skipped exon 2 and variably connected exon 1 to several possible downstream exons, collectively termed *CD22* Δex2* variants (Fig. 1C).

Further quantitative comparisons of TARGET pediatric B-ALL samples versus normal B cells using exon junction read counts revealed that *CD22* Δex5–6 is a cancer-selective isoform in pediatric B-ALL with minimal expression in normal B-cell types (Fig. 1D and E). In addition, the *CD22* Δex2* variants comprise over half of the *CD22* transcripts in many leukemias (Fig. 1F and G). To validate these isoforms, we performed RT-PCR on 18 primary diagnostic pediatric B-ALL samples previously obtained from the CHOP CCCR leukemia biorepository (29). By generating primers that spanned *CD22* exons 1 through 7, we validated the existence of Δex2, Δex2alt (which uses an alternative 3′ splice site in exon 3), Δex2–3, and the very common Δex5–6 and Δex2–6 isoforms using the B-ALL cell line Nalm6 (Fig. 1H; Sanger sequencing in Supplementary Table S1). *CD22* Δex2–4 was not visually detected,

Figure 1. Alternative splicing of *CD22* in human B-ALL. **A,** Quantification of LSVs across transcripts encoding major B-cell immunotherapeutic targets from pediatric B-ALL samples from the NCI TARGET consortium. **B,** *CD22* splice graph depicting splicing events across the 14 exons of *CD22* in B-ALL, with specific depiction of *CD22* Δex5–6 and *CD22* Δex2* variants. **C,** Relative frequencies of reads originating in exon 1 (blue numbers) or terminating in exon 7 (green numbers) in normal B-cell precursors (top) and B-ALL (bottom). **D** and **E,** Stack plots depicting relative abundance of *CD22* isoforms including/skipping exon 5 and 6 across TARGET dataset ($n = 219$) and normal B-cell subtypes ($n = 25$, from 11 individuals), respectively. BP, datasets corresponding to B-cell precursors obtained through the BLUEPRINT project; ped, pediatric samples. **F** and **G,** Stack plots depicting relative abundance of *CD22* Δex2* variants across TARGET dataset and normal B-cell subtypes, respectively. **H,** RT-PCR analysis validating *CD22* isoforms in the Nalm6 cell line. **I,** ONT-based long-read RNA-seq of *CD22* transcripts in cells from a *TCF3–HLF* B-ALL PDX model (ALL1807). *CD22* Δex5–6 and Δex2* variant transcripts are highlighted in yellow and purple, respectively.

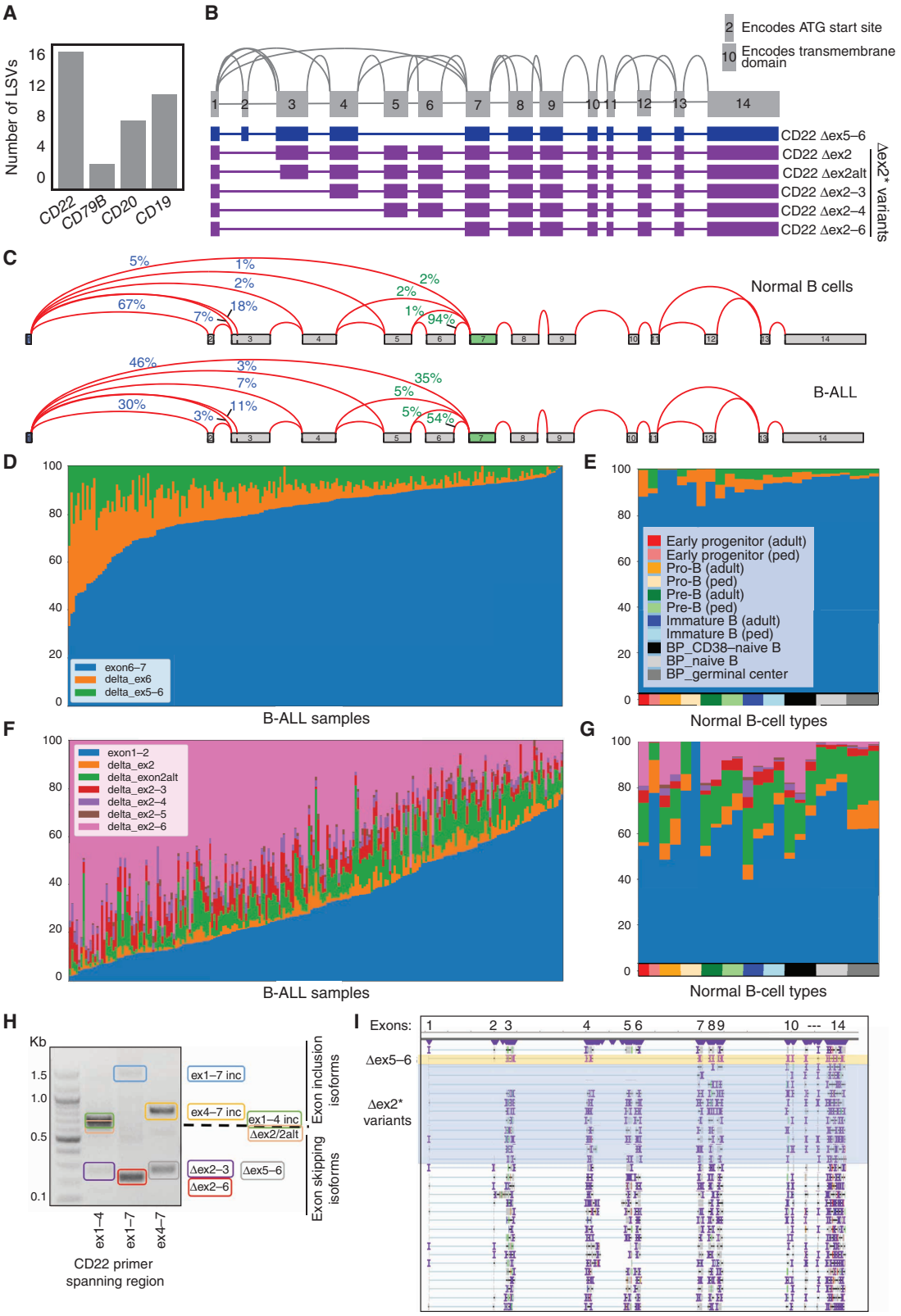

consistent with the low abundance of this isoform in the TARGET dataset. Finally, to demonstrate that exon 2- and exon 5–6-skipped splice variants could be detected as long polyadenylated transcripts, we performed Oxford Nanopore Technologies (ONT) long-read RNA-seq (30) on ALL1807, a patient-derived xenograft (PDX) model established from a pediatric patient with relapsed *TCF3-HLF*–driven B-ALL treated with and resistant to inotuzumab (31). We observed that skipping of 5′-terminal exons in this sample did not result in premature polyadenylation, with exon 14–derived sequences apparent in all reads (Fig. 1I).

CD22 Δex5–6 mRNA Isoform Encodes a Functional, HA22 Immunotherapy–Resistant Protein

To investigate the role of *CD22* splice isoforms in B-ALL further, we profiled *CD22* Δex5–6 mRNA expression by RT-PCR across a panel of primary pediatric B-ALL samples from the CHOP CCCR leukemia biorepository comprised of various genetic backgrounds. We detected *CD22* Δex5–6 expression in 16 of 18 assessed samples without obvious specificity for discrete B-ALL genetic subtypes (Fig. 2A). In the samples where *CD22* Δex5–6 was not detected, overall *CD22* gene expression was also notably low.

To determine whether this isoform can exist as a protein, we expressed the *CD22* Δex5–6 open reading frame ectopically. To this end, we deleted the endogenous *CD22* gene via CRISPR/Cas9 genome editing in the human B-cell lymphoma cell line OCI-Ly8 characterized by robust BCR signaling. We then reconstituted these CD22-negative cells with an empty retroviral vector, *CD22* Δex5–6, or canonical full-length *CD22* (*CD22 FL*). Both spliced isoforms were readily detectable by Western blotting using a conventional anti-CD22 antibody (Fig. 2B). However, endogenous CD22 Δex5–6 protein was not detectable by this technique in any of the 18 samples from Fig. 2A. To increase sensitivity, we immunoprecipitated reactive proteins from the lysates of several B-cell lines (Karpas422, Nalm6, and Reh) with a polyclonal CD22 antibody and then performed Western blotting using a different CD22 antibody. This two-step procedure yielded the dominant CD22 FL isoform and several minor bands, one of which corresponded to the size of CD22 Δex5–6 (Supplementary Fig. S2).

To demonstrate conclusively the existence of the endogenous CD22 Δex5–6 protein, we developed isoform-specific antibodies. We immunized BALB/c mice with a peptide spanning the junction between exons 4 and 7 (Fig. 2C) and generated a panel of monoclonal antibodies (mAb). To test these antibodies, we selected an array of cell lines and PDX models expressing *CD22* Δex5–6 mRNA as evidenced by RT-PCR (Fig. 2D). The majority of generated mAbs, exemplified by clone 11F11, exclusively recognized the engineered Δex5–6 isoform (Fig. 2E, left). Using 11F11, we detected immunoreactive bands of the expected size in both B-ALL cell lines (most prominently Reh, Fig. 2E, middle) and B-ALL PDXs (Fig. 2E, right). These experiments allowed us to conclude that endogenously expressed *CD22* Δex5–6 mRNA is translated into protein.

To elucidate the functional properties of CD22 Δex5–6, we performed flow cytometry on live cells using an antibody recognizing the N-terminus of all CD22 isoforms. We observed that both FL and Δex5–6 isoforms were readily detected on the cell surface (Fig. 2F). Consistent with being transported to the plasma membrane, the Δex5–6 isoform acquired the heavy glycosylation pattern of CD22 FL (32) as evidenced by the electrophoretic mobility shift after treatment with deglycosylating enzymes (Fig. 2G). Ligation of the BCR with an anti-IgM antibody leads to downstream signaling events such as BLNK phosphorylation (33, 34). While the loss of CD22 enhanced BCR signaling, both FL and Δex5–6 isoforms dampened phospho-BLNK levels (Fig. 2H and I). On the other hand, no effects of either isoform on cell viability were detected (Supplementary Fig. S3).

To explore the implications of CD22 Δex5–6 expression for CD22-targeted immunotherapies, we performed *in vitro* killing assays with HA22-based CAR T cells, whose single-chain variable fragment (scFv) was based on the RFB-4 antibody (35). This particular CAR construct was chosen for initial experiments because the HA22 CAR specifically recognizes the epitope encoded by *CD22* exon 5 (36, 37). Unlike the CD22 FL–expressing cells, CD22 Δex5–6 cells were inherently refractory to killing by the HA22 CAR (Fig. 2J). The same specificity was observed in killing assays with the prototype antibody RFB-4 combined with a drug-conjugated secondary antibody (Supplementary Fig. S4). This stood in contrast to the more commonly utilized m971 scFv–based CAR, which recognized a more membrane-proximal epitope than HA22 and demonstrated similar cytotoxicity against CD22 FL and Δex5–6 isoforms (Fig. 2K). On the basis of these data, we concluded that CD22 Δex5–6 could contribute to immunotherapeutic resistance, but such resistance would be restricted to agents that target the affected RFB-4/HA22 epitope.

CD22 Protein Expression *In Vitro* Is Limited by Exon 2 Inclusion

To identify broader mechanisms of immune escape, we tested whether *CD22* Δex2* variants missing the initiation codon could mediate antigen escape through downmodulation of total CD22 protein output. As predicted, after reconstituting CD22-deleted OCI-Ly8 cells with CD22 FL and CD22 Δex2–6, only the cells expressing CD22 Δex2–6 failed to show any flow cytometric staining by multiple anti-CD22 antibodies (Fig. 3A). The same negative result was observed when cells expressing the vesicular stomatitis virus G protein (VSVg)–tagged form of CD22 Δex2–6 were stained with an anti-VSVg antibody (Supplementary Fig. S5). We were

Figure 2. Biochemical and functional characterization of the CD22 Δex5–6 isoform. **A,** RT-PCR detection of *CD22* Δex5–6 across 18 diagnostic *de novo* B-ALL samples driven by various genetic alterations. **B,** Western blotting using N-terminus–directed anti-CD22 antibody performed on *CD22*-deleted OCI-Ly8 cells engineered to express *CD22* Δex5–6 or FL isoforms. KO, knockout. **C,** Amino acid sequence of the peptide used for mAb production. **D,** RT-PCR detection of *CD22* Δex5–6 in OCI-Ly8 cell lines from **B**, human B-ALL cell lines, and B-ALL PDXs. **E,** Western blotting using the 11F11 mAb performed on cells from **D**. **F,** Flow cytometric detection of CD22 KO, CD22 FL, and CD22 Δex5–6. FSC-A, forward scatter area. **G,** Western blotting demonstrating electrophoretic mobilities of CD22 isoforms treated with deglycosylating enzymes with or without denaturation. **H,** Western blotting detecting CD22 and total and phosphorylated (p) BLNK in derivatives from **B** treated with an anti-IgM antibody for indicated time intervals. **I,** Quantitation of pBLNK bands from **H**. The experiment was replicated twice with concordant results. **J** and **K,** *In vitro* killing assays performed on cells from **B** using HA22- and m971-based CD22 CAR T cells (CART22), respectively ($n = 2$ technical replicates). Data in both panels are represented as mean values ± SD error bars.

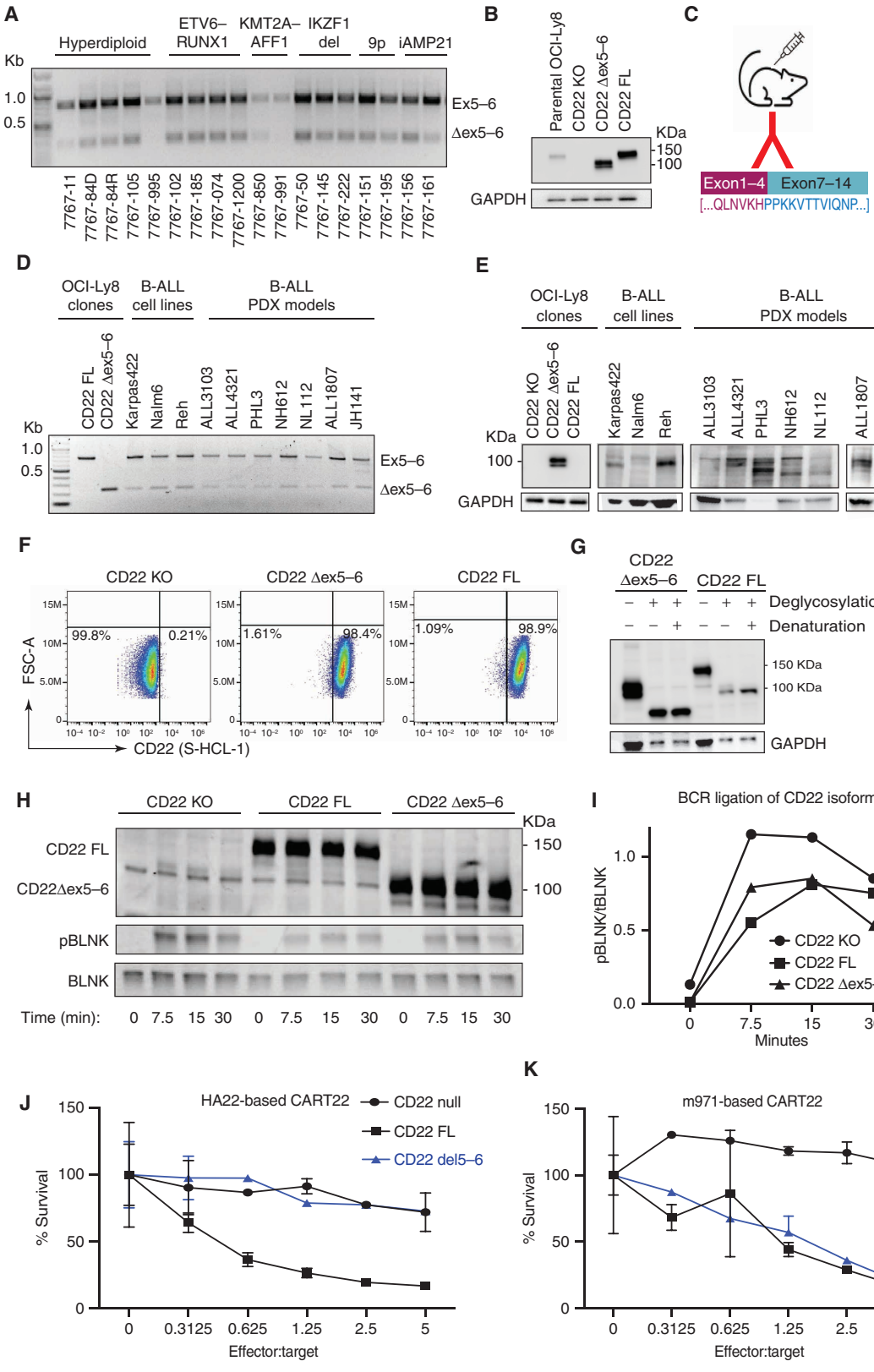

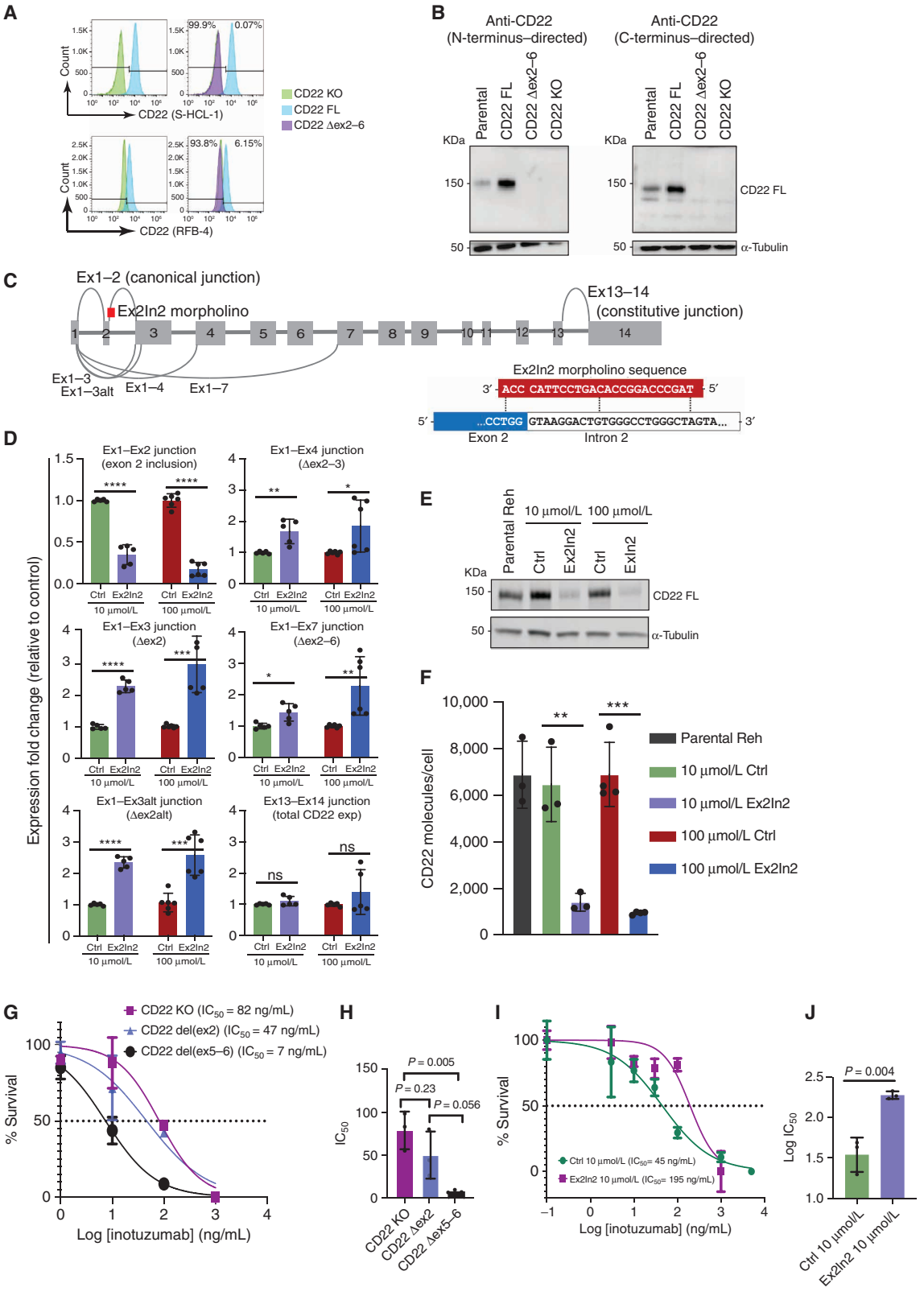

unable to identify any protein products corresponding to CD22 Δex2–6 by Western blotting, even when probed with the anti-CD22 antibody recognizing its intracellular C-terminus (Fig. 3B; Supplementary Fig. S6).

To confirm further that loss of exon 2 precludes *CD22* mRNA translation, we designed a morpholino antisense oligonucleotide spanning the junction between exon 2 and intron 2 to interfere with exon 2 inclusion (Fig. 3C). Indeed, when this splice site blocker was transfected into Reh B-ALL cells at 10 μmol/L and 100 μmol/L concentrations, the total *CD22* mRNA levels did not change (as measured by the expression of the constitutive exon junction *CD22* ex13–14), but the ratio of exon 2–skipping to exon 2–including isoforms increased in a dose-dependent manner (Fig. 3D; Supplementary Table S2). Although we saw the greatest increase in Δex2 and Δex2alt expression, the morpholino induced expression of the other *CD22* Δex2* variants as well (Fig. 3D). Accordingly, the CD22 protein output as measured by Western blotting and quantitative flow cytometry (Fig. 3E and F, respectively) was reduced to one seventh that of parental cells using the 100 μmol/L morpholino concentration. Together, these results show that *CD22* Δex2* transcripts do not utilize alternative start codons and are in essence noncoding.

We then set out to determine whether exon 2 skipping contributes to increased resistance to inotuzumab ozogamicin, an immunoconjugate based on the humanized version of the m5/44 antibody recognizing the very N-terminus of CD22 (38). We predicted that cells expressing *CD22* Δex5–6 should remain sensitive to inotuzumab, but cells expressing *CD22* Δex2* variants should acquire some degree of resistance to the drug. Indeed, in cell viability assays utilizing inotuzumab, IC_{50} curves corresponding to *CD22* Δex2–expressing and *CD22* knockout (KO) cells were indistinguishable from each other but attested to decreased sensitivity (1-log rightward shift) compared with the IC_{50} curves generated for *CD22* Δex5–6 cells (Fig. 3G and H). Most importantly, treating Reh B-ALL cells with the morpholino exon 2 splice site blocker also resulted in increased resistance to inotuzumab (Fig. 3I and J).

CD22 Protein Expression on Leukemic Blasts Is Limited by Exon 2 Inclusion in Patients with B-ALL on the AALL1621 Phase II Inotuzumab Clinical Trial

To extend our biochemical observations to a relevant clinical setting, we obtained 22 B-ALL bone marrow or peripheral blood samples from pediatric patients who were treated with inotuzumab on the Children's Oncology Group (COG) AALL1621 phase II clinical trial (NCT02981628; Supplementary Table S3). Included in the samples were paired specimens from four patients who subsequently relapsed after inotuzumab treatment with at least 5% residual disease. Of these patients, two demonstrated concurrent downregulation of CD22 surface expression with loss of response to inotuzumab, and one patient failed to have an initial response to inotuzumab. We measured *CD22* RNA levels using qRT-PCR and RNA-seq and quantified the median number of surface CD22 molecules per cell via flow cytometric site density assays (39). We observed that while CD22 cell surface protein expression did not correlate with total *CD22* transcript levels (Fig. 4A, left), it did correlate with expression levels of the *CD22* exon 2–including isoform (Fig. 4A, right). This phenomenon suggested that exon 2 inclusion is rate limiting for CD22 protein expression.

To evaluate the possible role of *CD22* exon 2 skipping in inotuzumab resistance, we performed deep RNA-seq and splicing analysis of pretreatment primary cells from patients enrolled on AALL1621. Once again, we noted the frequent skipping of *CD22* exons 5 and 6 (Supplementary Fig. S7), while Δex2–6 was by far the most prevalent and abundant isoform among the Δex2* variants (Fig. 4B), approximately matching the prevalence of *CD22* Δex2–6 in the TARGET dataset (Fig. 1F). In one patient (PAYYZW, Fig. 4B, yellow arrow), this was the only *CD22* isoform expressed at detectable levels, and not surprisingly, this patient had failed to respond to inotuzumab. Hence, prominent expression of the *CD22* Δex2–6 isoform in primary leukemias may create the potential for splicing-based *de novo* resistance in some patients.

We then focused on three pediatric B-ALL cases with significant downregulation of surface CD22 during disease progression after inotuzumab therapy. In the first patient (PAWUXD), we observed a two-thirds reduction in CD22 surface expression from pretreatment to posttreatment specimens as measured by flow cytometry (Fig. 4C; Supplementary Fig. S8). When we performed RNA-seq–based mutation calling, we discovered a *de novo* AA>GG mutation at the junction between exon 2 and intron 2 in 27% of reads in the post-inotuzumab relapse sample. This two-nucleotide substitution alters the 5′ splice site from the canonical GTAAGT to the less favorable GTGGGT hexad at intronic positions +1 to +6 (Fig. 4D). We hypothesize that this substitution could contribute to frequent skipping of exon 2, although downregulation of CD22 protein in this sample was largely

Figure 3. CD22 protein expression in B-cell malignancies is limited by exon 2 inclusion. **A,** Flow cytometric detection of exogenously expressed CD22 protein in *CD22*-deleted OCI-Ly8 cells using anti-CD22 antibodies directed toward either the extreme N-terminus (S-HCL-1) or the C-terminal region (RFB-4) of the extracellular domain. KO, knockout. **B,** Western blotting detection of CD22 in the same cell lines and parental controls using anti-CD22 antibodies directed toward the N-terminus (R&D Systems, MAB19681) and the C-terminus (Boster Bio, PB9691). **C,** Schematic annotating the *CD22* exon splice junctions (gray arches) assayed using junction-spanning qPCR primers following treatment with Ex2In2 morpholino. Bottom right, morpholino sequence is shown in red, with complementary exon–intron junction sequence shown in blue/white. **D,** qRT-PCR detection of various *CD22* mRNA isoforms in Reh B-ALL cells transfected for 48 hours with Ex2In2 (10 μmol/L and 100 μmol/L). Constitutive expression of ex13–14 junction was used as a measure of total *CD22* expression ($n = 6$, 2 independent experiments with 3 technical replicates each). *, $P < 0.05$; **, $P < 0.01$; ***, $P < 0.001$; ****, $P < 0.0001$. ns, not significant. **E** and **F,** Detection of CD22 protein in the morpholino-treated Reh cells by Western blotting and flow cytometric site density assay, respectively ($n = 2$ independent experiments). **G,** Viability assay performed on *CD22*-deleted OCI-Ly8 cells reconstituted with indicated *CD22* isoforms and treated for 24 hours with indicated concentrations of inotuzumab ($n = 3$ technical replicates). IC_{50} 95% confidence intervals (CI) were as follows: 54–119 ng/mL for CD22 KO, 25–85 ng/mL for CD22 Δex2, and 5–11 ng/mL for CD22 Δex5–6. **H,** Bar graph representing IC_{50} values from **G**. *P* values were determined using an unpaired *t* test. **I,** Viability assay performed on Ex2In2-treated (48 hours) and inotuzumab-treated (24 hours) Reh cells ($n = 3$ technical replicates). Cell viability was assessed using the WST-1 assay. IC_{50} 95% CIs were 29–72 ng/mL for Ctrl treatment and 119–333 ng/mL for Ex2In2 treatment. **J,** Bar graph representing IC_{50} values from **I** on the log scale. *P* values were determined using an unpaired *t* test. Data in **D**, **F**, **H**, and **J** are presented as individual and mean values ± SD error bars. Data in **G** and **I** are presented as mean values ± SD error bars.

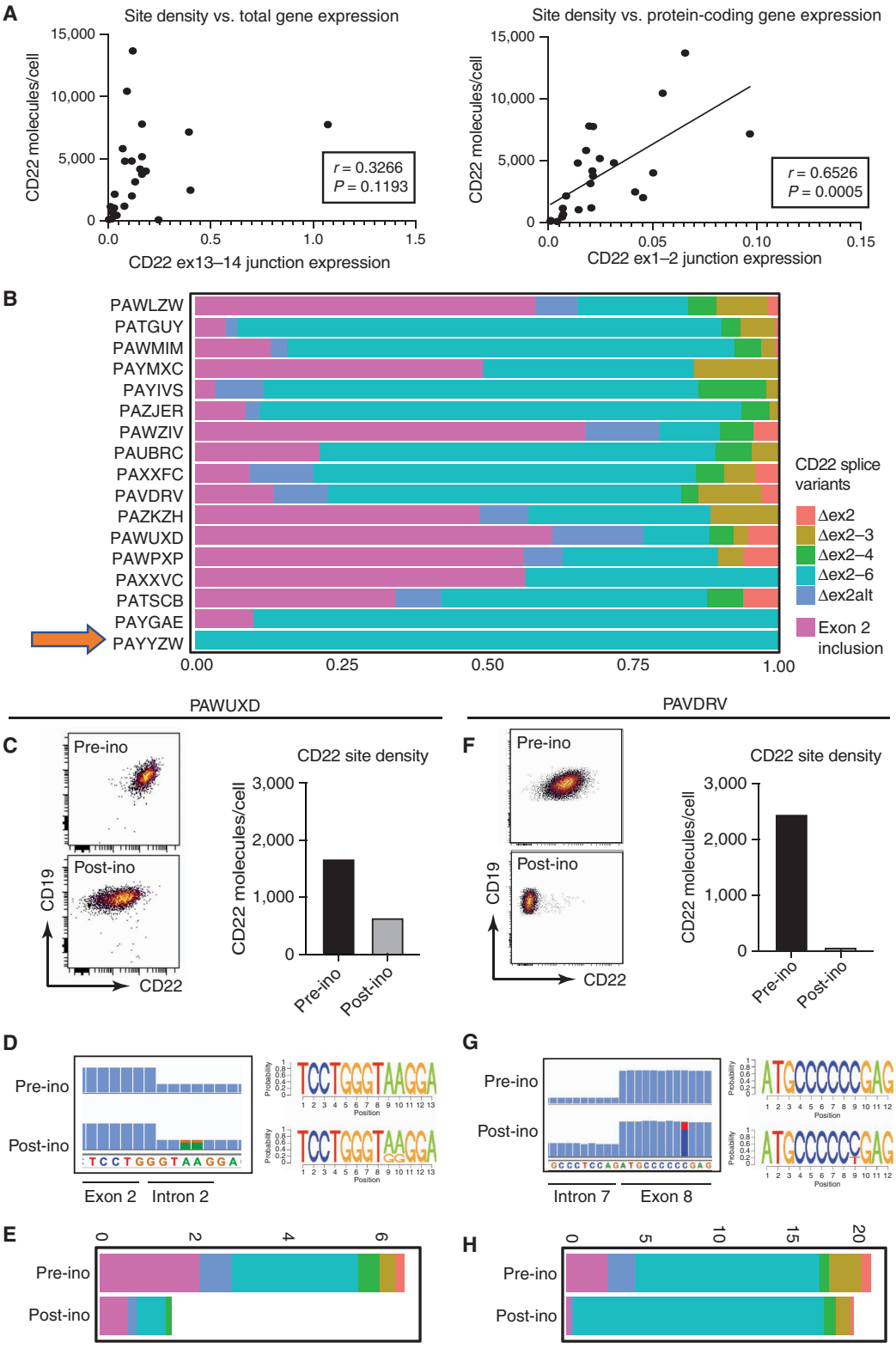

concordant with the decrease in total *CD22* RNA-seq read counts (Fig. 4E). A similar pattern of CD22 protein changes was also observed in serial B-ALL bone marrow samples from a child with recurrently relapsed B-ALL treated at the Children's Hospital of Philadelphia (CHOP) with commercially available inotuzumab outside of the AALL1621 trial. Namely, we detected decreased B-ALL cell–specific CD22 protein levels after an incomplete clinical response to inotuzumab and subsequent recovery of CD22 expression upon completion of immunotherapy (Supplementary Fig. S9A); the *CD22* RNA levels closely followed the same trend (Supplementary Fig. S9B). This concordance between CD22 mRNA and protein levels was indicative of a predominantly transcriptional mechanism of antigen downmodulation.

However, in a second set of paired pre- and post-inotuzumab specimens from the AALL1621 patient PAVDRV, we detected an approximately 99% reduction in surface CD22 (Fig. 4F; Supplementary Fig. S8) without a commensurate downregulation of the *CD22* transcript. In 22% of reads, we discovered a *de novo* C>T mutation in exon 8 introducing a premature TGA stop codon (Fig. 4G). However, as this mutation was subclonal, it was unlikely to be a dominant means of CD22 protein downregulation. We also found an acquired subclonal mutation (26% reads) in the 5′ splice site of exon 4 (G>A at intronic position +1), which could contribute to *CD22* AS, in particular to the apparent increase in *CD22* Δex5–6 usage (Supplementary Fig. S10A and S10B). While we did not observe alterations in the 5′ or 3′ splice sites surrounding exon 2, there was a profound shift from exon 2–including (purple) to exon 2–6-skipping (teal) isoforms (Fig. 4H), sharply reducing the amount of translatable *CD22* mRNA. These discoveries directly implicate AS of *CD22* in resistance to CD22-directed immunotherapy.

DISCUSSION

Herein, we present evidence supporting the role of AS in mediating resistance to CD22-targeted therapies in patients with B-ALL. These events fall into two broad categories defined by skipping of *CD22* exons 5–6 or exon 2 (alone or with the downstream exons). In the first case, we show that the Δex5–6 event preserves surface localization, maintains the functional intracellular domain of CD22, and does not diminish sensitivity to anti-CD22 m971 CAR T cell immunotherapy in *in vitro* assays. However, the Δex5–6 AS event does result in loss of the RFB-4 epitope, with ensuing resistance to RFB-4–based immunotherapeutics such as HA22 CAR T cells and the RFB-4 antibody itself when combined with a secondary antibody–drug conjugate. While HA22 is not being developed further in the clinic, the RFB-4/HA22-based immunoconjugate moxetumomab pasudotox is FDA approved for the treatment of patients with hairy cell leukemia (40, 41). Interestingly, moxetumomab did not show appreciable efficacy in children with relapsed B-ALL in a phase II clinical trial (42), and we speculate that *CD22* Δex5–6 may have played a role in this failure.

Of even broader significance could be the pervasive skipping of *CD22* exon 2 in which the open reading frame starts. This AS event limited the amount of translatable *CD22* transcripts in two independent cell lines (as shown in the morpholino experiments) and in primary patient ALL specimens. Most importantly, the forced switching from protein-coding to noncoding Δex2* variants conferred resistance to inotuzumab *in vitro*. This could be highly relevant in clinical settings, as the *CD22* Δex2–6 isoform was prevalent in many AALL1621 diagnostic samples. In the most extreme case (PAYYZW), Δex2–6 was the *only* detectable CD22 isoform, which correlated with the lack of response to inotuzumab. Even in less extreme cases, the near-ubiquitous presence of Δex2* variants in B-ALL specimens suggests that some patients could already be primed to develop rapid splicing-mediated antigen escape at diagnosis. This appears to be the case with patient PAVDRV, wherein AS was the predominant form of dysregulation of the *CD22* transcript, as opposed to subclonal nonsense mutations described previously for *CD19* (7, 9, 11). On the other hand, leukemias with moderate preexisting dysregulation of splicing, such as PAWUXD, may be more dependent on transcriptional mechanisms such as epigenetic silencing.

Our discovery of *de novo* mutations within relevant splice junctions further elucidates a possible means by which splicing changes occur. Interestingly, exon 2 splice site mutations were observed in the relapse sample that had not demonstrated significant AS-mediated antigen escape. Conversely, they were not detectable by RNA-seq in the relapse sample with strong evidence of AS-associated escape, suggesting that CD22 splicing dysregulation can occur by both "slow" mutational and "fast" nonmutational mechanisms, such as well-documented dysregulation of RNA-binding proteins (43). The recent emergence of inotuzumab as a potential first-line therapeutic agent for patients with B-ALL (15) will undoubtedly provide additional specimens for experimental study to elucidate the molecular mechanisms of *CD22* AS. Then molecular determinants of *CD22* AS could become useful predictive biomarkers, similar to splicing polymorphisms in *CD33* that are implicated in responses to gemtuzumab, a CD33 immunoconjugate, in patients with acute myeloid leukemia (44). And if splicing aberrations prove to be druggable, they could provide novel

Figure 4. CD22 protein expression is limited by exon 2 inclusion in B-ALL cells. **A,** Correlation analysis of CD22 site density versus *CD22* mRNA levels in pretreatment primary B-ALL bone marrow or peripheral blood specimens obtained from children enrolled on the COG AALL1621 phase II clinical trial. *CD22* mRNA levels were measured by qRT-PCR using primers specific for the exon 13–14 (left) or exon 1–2 (right) junctions. *CD22* expression was normalized to that of β-actin. Regression coefficients and *P* values are shown for each comparison. **B,** Relative expression of *CD22* exon 2–containing and exon 2–skipping splice variants within baseline AALL1621 B-ALL specimens. Each stack plot represents a single patient (designated by the COG unique specimen identifier). Yellow arrow highlights PAYYZW as a sample apparently devoid of protein-coding *CD22* mRNA isoforms. The legend shows color-coded *CD22* splice variants. **C,** Flow cytometric quantitation of CD22 molecules in paired pre– and post–inotuzumab treatment (pre-ino/post-ino) bone marrow specimens from AALL1621 patient PAWUXD with multiply relapsed B-ALL. **D,** *CD22* mutational analysis of the paired PAWUXD samples. **E,** *CD22* exon 2 splicing analysis of the paired PAWUXD samples. For color coding, refer to legend in **B**. **F,** Flow cytometric quantitation of CD22 molecules in paired pre- and posttreatment (pre-ino/post-ino) bone marrow specimens from AALL1621 patient PAVDRV with multiply relapsed B-ALL. **G,** *CD22* mutational analysis of the paired PAVDRV samples. **H,** *CD22* exon 2 splicing analysis of the paired PAVDRV samples. For color coding, refer to legend in **B**.

means to achieve robust and stable expression of CD22 and sustained responses to antibody- and cell-based CD22-directed immunotherapies.

METHODS

Human Primary ALL Specimens and PDX Models

Patients treated with inotuzumab on the AALL1621 trial (NCT02981628) received one or more cycles of the drug administered as 0.8 mg/m^2 on day 1, 0.5 mg/m^2 on day 8, and 0.5 mg/m^2 on day 15 (20). Disease evaluations were conducted at study entry prior to inotuzumab administration, on day 28 of each cycle after inotuzumab treatment, or at alternative time points as clinically indicated. Viably cryopreserved Ficoll gradient–purified mononuclear cells from primary bone marrow or peripheral blood from children with relapsed/refractory B-ALL were obtained via written informed consent on Institutional Review Board–approved research protocols of COG and CHOP in accordance with the Declaration of Helsinki. Primary ALL cells were thawed for downstream flow cytometry analysis (described below) or subjected to nucleic acid extraction using Qiagen RNeasy kits for qRT-PCR and RNA-seq analysis. Pediatric ALL PDX modeling of some samples was performed as described previously (31, 45, 46). All animal studies were approved by the CHOP Institutional Animal Care and Use Committee.

Dataset Usage

We accessed RNA-seq data from the TARGET ALL phase I and II projects (https://portal.gdc.cancer.gov/projects) and from the BLUEPRINT consortium (http://dcc.blueprint-epigenome.eu). TARGET ALL data used for this analysis were accessed under project #10088: "Alternative splicing in pediatric cancers" (request 41466-5).

RNA-seq Analysis

RNA-seq reads were first trimmed to remove adapters (BBTools version 38.87) and were then aligned using STAR version 2.7.3a to the hg38 reference genome while providing known gene isoforms through the GENCODE annotation version 32. In addition, we used STAR flags "–quantMode GeneCounts" and "–alignSJoverhangMin 8" to quantify genes and ensure spliced reads had an overhang of at least eight bases. Junction spanning reads were obtained from the STAR "*_SJ.out.tab" result files, and each entry was normalized by dividing by the total number of junction-spanning reads and multiplying by a factor of 1 million. Visualization and downstream analyses were conducted in R using the ggplot2 and tidyverse packages. Single-nucleotide variations, insertions, and deletions were identified using the SAMtools (47) and BCFtools (48) packages.

MAJIQ Splicing Analysis

The MAJIQ algorithm (28) was run with each sample being quantified individually on a build comprising 219 TARGET B-ALL samples with *de novo* junction detection but without intron retention detection. Samples were run against the Ensembl hg38 GFF3 annotation (v94) and required a minimum of five reads per sample per junction for quantification. For the splice graphs showing average junction quantification in CD22, a second MAJIQ build was used, comparing the B-ALL group (TARGET samples) against the B-cell subtypes (derived from seven healthy donors from BLUEPRINT and four healthy donors from the CHOP CCCR biorepository).

qRT-PCR

Total RNA was isolated using the Qiagen RNeasy kit and reverse transcribed using SuperScript IV (Invitrogen; 18090010). Primers used for each *CD22* mRNA isoform are listed in Supplementary Table S2. qRT-PCR was performed using PowerSYBR Green PCR Master Mix (Life Technologies). Reactions were performed on an Applied Biosystems Viia7 machine and analyzed with Viia7 RUO software (Life Technologies). When indicated, individual PCR products were gel purified (QIAquick Gel Extraction Kit; Qiagen) and Sanger sequenced.

ONT Long-read Sequencing

Total RNA was extracted from the ALL1807 PDX model sample (31) using the Qiagen RNeasy kit following manufacturer's instructions. The mRNA was isolated from 100 μg of total RNA using Dynabeads mRNA DIRECT kit (Invitrogen) and subjected to direct RNA (SQK-RNA002, ONT) library preparation. Subsequently, each library was loaded into a Spot-ON Flow Cell R9 version (FLO-MIN106D, ONT) and sequenced in a MinION Mk1B device (ONT) for 48 hours. Raw Fast5 files were converted to fastq with guppy (v3.4.5), followed by alignment to the gencode version of hg38 (v30) using minimap2 (v2.18); the resulting bam file was visualized using the Integrative Genomics Viewer (v2.9.0).

Quantitative Flow Cytometry and Antigen Site Density Analysis

Viably cryopreserved B-ALL patient specimens from the COG AALL1621 trial were used for single-cell flow cytometry analysis of viability and CD22 site density as described previously (39) using a FACSVerse flow cytometer (BD Biosciences). Human B-ALL samples were stained with Fc block (BioLegend; #422301), Zombie Aqua viability dye (BioLegend; #423101), and PE-conjugated anti-CD22 (BD Biosciences; #347577); Quantibrite beads (BD Biosciences; #340495) were used to enumerate CD22 molecules/cell.

Cell Lines and Cell Culture

Human diffuse large B-cell lymphoma OCI-Ly8 and B-ALL Reh cell lines were cultured and maintained in RPMI1640 medium supplemented with 10% FBS, 2 mmol/L L-glutamine, and antibiotic–antimycotic at 37°C and 5% CO_2. The use of Reh cells has been described previously (29). The OCI-Ly8 cell line was a kind gift from the laboratory of Raju Chaganti (Memorial Sloan Kettering Cancer Center, New York, NY). Cell line authentication for OCI-Ly8 and Reh was performed by short tandem repeat profiling in 2021. All cell lines were routinely confirmed to be *Mycoplasma* free via Sartorius EZ-PCR Mycoplasma Detection Kit.

Genome Editing

CD22-CRISPR/Cas9-KO plasmid (using a cocktail of single-guide RNAs homologous to exons 3 and 5) was obtained from Santa Cruz Biotechnology and transfected into OCI-Ly8 cells via electroporation using the AMAXA system program 0–006 and Reagent V (Lonza). CD22-deficient cells were sorted 4 days after transfection and plated individually in 96-well clusters for single-cell clone selection and expansion. CD22 knockdown was confirmed by flow cytometry and Western blotting. CD22 FL, CD22 FL-VSVg (with VSVg tag placed in exon 2 after the signal peptide), CD22 Δex2–6, CD22 Δex2–6-VSVg (with VSVg tag placed in exon 7 after putative ATG site and signal peptide), CD22 Δex5–6, and CD22 Δex5–6-VSVg (with VSVg tag placed in exon 2) were synthesized and cloned into the pMXs-IRES-Blasticidin retroviral vector. *CD22*-deleted cells were reconstituted with retroviral vector pMXs-IRES-Blasticidin bearing no insert ("empty vector") or the constructs described above. Selection of infected cells was performed with 10 μg/mL blasticidin over the course of 1 week.

BCR Ligation

BCR ligation was performed by incubating 2×10^7 cells with 10 μg/mL of pre-BCR–specific α-IgM Jackson ImmunoResearch antibody for indicated time points at room temperature as described previously (33).

Deglycosylation Assay

Whole-cell protein lysates were obtained and treated with a deglycosylation mix in denaturing and nondenaturing buffers (New England BioLabs; #P6039S) in the presence of protease and phosphatase inhibitors (Thermo Scientific; #78446) following manufacturers' instructions. Control and deglycosylated lysates were loaded onto 7.5% NuPAGE gels for Western blotting analysis.

Western Blotting and Immunoprecipitation

For Western blotting, cells were lysed in RIPA buffer and loaded on 7.5% or 10% NuPAGE gels. For detection of murine and human proteins, primary human anti-CD22 antibodies (Boster Bio, PB9691; R&D Systems, MAB19681) were used in combination with anti-rabbit or anti-mouse horseradish peroxidase–linked secondary antibodies (Cell Signaling Technology) and Amersham Enhanced Chemiluminescence Western Blotting Detection Reagent (GE Life Sciences). Immunoprecipitation was performed on precleared whole-cell lysates in nondenaturing NP-40 lysis buffer. After overnight incubation with primary antibody at 4°C, protein A agarose beads were added to lysate and incubated for 1 hour at 4°C. Beads were washed three times in lysis buffer, and proteins were eluted in Laemmli sample buffer for further Western blotting analysis.

In Vitro *CAR T Cell Killing Assay*

OCI-Ly8 Δ*CD22* cells expressing CD22 FL, CD22 Δex5–6, or empty vector together with pELNS-CBR-T2A-GFP were used as targets for T-cell cytotoxicity assay as described previously (9). Briefly, target cells were incubated with effector T cells (CD22 CAR T cells) at the indicated effector-to-target cell ratios for 24 hours. D-luciferin (Goldbio; #LUCK-1G) was then added to the cell culture, and bioluminescence imaging was performed on a Xenogen IVIS-200 Spectrum camera. Target killing was analyzed using the software Living Image 4.3.1 (Caliper LifeSciences).

Morpholino Treatment

Control and Ex2In2 morpholinos (1 mmol/L stock concentration; see Supplementary Table S2) were electroporated into 1×10^6 Reh cells via the Neon transfection system using concentrations of 10 μmol/L and 100 μmol/L in 2-mL suspensions. Cells were seeded in triplicate in a 6-well plate. After 48 hours, cells were harvested for protein and RNA to conduct Western blotting and qRT-PCR. Aliquots of live cells were also saved to conduct CD22 site density analysis.

In Vitro *Inotuzumab Killing Assay*

OCI-Ly8 Δ*CD22* cells expressing CD22 FL or CD22 Δex5–6 were seeded in triplicate at 2×10^5 cells in 100 μL of RPMI at specified concentrations of inotuzumab in a 96-well plate. After 48 hours of incubation, cell viability was assayed via CellTiter-Glo (Promega) as per manufacturer's instructions. Bioluminescence was analyzed using BioTek Synergy 2. Morpholino-treated Reh cells incubated with inotuzumab for 48 hours as described above were assayed for cell viability using the WST-1 cell proliferation reagent according to the manufacturer's protocol (Sigma-Aldrich; 05015944001). Absorbance was measured using the BioTek Synergy 2 instrument.

Data Availability

RNA-seq data generated for the PAWUXD and PAVDRV paired specimens are deposited at the NCBI Sequence Read Archive and can be accessed online with the BioProject ID PRJNA764243. Gene expression data for the remaining primary COG AALL1621 specimens referenced in the article are included in Supplementary Gene Expression Data.

Authors' Disclosures

S. Zheng reports grants from Ruth L. Kirschstein National Research Service Award (NRSA; Institutional Research Training Grants; T32) during the conduct of the study, as well as a patent for antibodies for the diagnosis and treatment of B-cell acute lymphoblastic leukemia pending. E. Gillespie reports grants from T32 CA115299 during the conduct of the study, as well as other support from Inovio Pharmaceuticals, Inc. outside the submitted work. D.A. Hottman reports other support from Nuventra, LLC outside the submitted work. D.M. Taylor reports personal fees from AstraZeneca outside the submitted work. S.R. Rheingold reports other support from Pfizer outside the submitted work. M.M. O'Brien reports grants from Pfizer and NCI during the conduct of the study, as well as grants and nonfinancial support from AbbVie, Amgen, and Pfizer, personal fees from Jazz, and nonfinancial support from Celgene outside the submitted work. N. Singh reports personal fees from Aerpio Pharmaceuticals outside the submitted work, as well as a patent for 62/149,249 licensed to University of Pennsylvania, a patent for 62/722,486 pending, and a patent for 63/136,702 pending. M. Ruella reports other support from Novartis/Penn during the conduct of the study; personal fees from Bristol Myers Squibb, GlaxoSmithKline, and Sana and grants and personal fees from AbClon outside the submitted work; and patents for US10253086B2 and US11026976B2 issued, licensed, and with royalties paid from Novartis. Y. Barash reports grants from NIH during the conduct of the study. The MAJIQ software used in this study is available for licensing for free for academics and for a fee for commercial usage. Some of the licensing revenue goes to Y. Barash and members of the Barash lab. S.K. Tasian reports grants from NCI, Department of Defense, St. Baldrick's Foundation–Stand Up To Cancer, Gilead Sciences, Beam Therapeutics, and V Foundation for Cancer Research during the conduct of the study, as well as grants and nonfinancial support from Incyte Corporation, and personal fees from Aleta Biotherapeutics and Kura Oncology outside the submitted work. A. Thomas-Tikhonenko reports grants from NCI, Pfizer ASPIRE Program, St. Baldrick's Foundation–Stand Up To Cancer, V Foundation for Cancer Research, Cookies for Kids' Cancer Foundation, and Abramson Cancer Center at the University of Pennsylvania during the conduct of the study; personal fees from Guidepoint, Qatar National Research Fund, NIH, and University of Miami outside the submitted work; and a patent for PCT/US2020/043939 pending and a patent for US20170239294A1 issued. No disclosures were reported by the other authors.

Authors' Contributions

S. Zheng: Conceptualization, data curation, formal analysis, investigation, writing–original draft, writing–review and editing. **E. Gillespie:** Conceptualization, investigation. **A.S. Naqvi:** Conceptualization, data curation, formal analysis. **K.E. Hayer:** Data curation, software, formal analysis, visualization. **Z. Ang:** Investigation. **M. Torres-Diz:** Investigation. **M. Quesnel-Vallieres:** Data curation, formal analysis, visualization. **D.A. Hottman:** Investigation. **A. Bagashev:** Investigation. **J. Chukinas:** Investigation. **C. Schmidt:** Data curation, software, formal analysis, investigation. **M. Asnani:** Investigation. **R. Shraim:** Data curation, software, formal analysis, investigation. **D.M. Taylor:** Formal analysis, supervision. **S.R. Rheingold:** Resources, funding acquisition. **M.M. O'Brien:** Resources, supervision. **N. Singh:** Investigation. **K.W. Lynch:** Conceptualization, supervision. **M. Ruella:** Conceptualization, data curation, supervision. **Y. Barash:** Conceptualization, data curation, software, supervision. **S.K. Tasian:** Conceptualization, resources, supervision, writing–review and editing. **A. Thomas-Tikhonenko:** Conceptualization, resources, supervision, writing–original draft, writing–review and editing.

Acknowledgments

This work was supported by grants from the NIH (U01 CA232563 and U01 CA232563-S2, to A. Thomas-Tikhonenko, Y. Barash, and

K.W. Lynch; U01 CA232486 and U01 CA243072, to S.K. Tasian; K99/R00 CA212302, to M. Ruella; T32 CA009615, to S. Zheng; and T32 CA115299, to E. Gillespie and A.S. Naqvi), the Department of Defense (CA180683P1, to S.K. Tasian), Pfizer's ASPIRE Oncology/Hematology Research Program (to A. Thomas-Tikhonenko, S.R. Rheingold, and M.M. O'Brien), St. Baldrick's–Stand Up To Cancer (SU2C-AACR-DT-27-17, to A. Thomas-Tikhonenko and S.K. Tasian), Stand Up To Cancer (Philip A. Sharp Award for Innovation in Collaboration Award, grant number SU2C-AACR-PS-27, to S.K. Tasian), the V Foundation for Cancer Research (Translational Grant, to S.K. Tasian; T2018-014, to A. Thomas-Tikhonenko), and Cookies for Kids' Cancer (CFKC) Foundation (to A. Thomas-Tikhonenko) and philanthropy for leukemia research from the Simutis family in memory of Andrew David Simutis. COG and institutional primary leukemia specimen banking were supported by NCI U24 CA114766 and U24 CA196173. M. Ruella, S.K. Tasian, and A. Thomas-Tikhonenko are members of the Abramson Cancer Center (ACC), and A. Thomas-Tikhonenko is Richard "Buz" Cooper Scholar of the ACC-Breakthrough Bike Challenge. Stand Up To Cancer is a division of the Entertainment Industry Foundation. The indicated SU2C grants are administered by the American Association for Cancer Research, the scientific partner of SU2C.

Received May 31, 2021; revised September 30, 2021; accepted November 10, 2021; published first November 12, 2021.

REFERENCES

1. Roberts KG, Mullighan CG. Genomics in acute lymphoblastic leukaemia: insights and treatment implications. Nat Rev Clin Oncol 2015;12:344–57.
2. Aldoss I, Bargou RC, Nagorsen D, Friberg GR, Baeuerle PA, Forman SJ. Redirecting T cells to eradicate B-cell acute lymphoblastic leukemia: bispecific T-cell engagers and chimeric antigen receptors. Leukemia 2016;31:777–87.
3. Topp MS, Gokbuget N, Stein AS, Zugmaier G, O'Brien S, Bargou RC, et al. Safety and activity of blinatumomab for adult patients with relapsed or refractory B-precursor acute lymphoblastic leukaemia: a multicentre, single-arm, phase 2 study. Lancet Oncol 2015;16:57–66.
4. Maude SL, Frey N, Shaw PA, Aplenc R, Barrett DM, Bunin NJ, et al. Chimeric antigen receptor T cells for sustained remissions in leukemia. N Engl J Med 2014;371:1507–17.
5. Gardner R, Wu D, Cherian S, Fang M, Hanafi LA, Finney O, et al. Acquisition of a CD19-negative myeloid phenotype allows immune escape of MLL-rearranged B-ALL from CD19 CAR-T-cell therapy. Blood 2016;127:2406–10.
6. Jacoby E, Nguyen SM, Fountaine TJ, Welp K, Gryder B, Qin H, et al. CD19 CAR immune pressure induces B-precursor acute lymphoblastic leukaemia lineage switch exposing inherent leukaemic plasticity. Nat Commun 2016;7:12320.
7. Asnani M, Hayer KE, Naqvi AS, Zheng S, Yang SY, Oldridge D, et al. Retention of CD19 intron 2 contributes to CART-19 resistance in leukemias with subclonal frameshift mutations in CD19. Leukemia 2020;34:1202–7.
8. Bagashev A, Sotillo E, Tang CH, Black KL, Perazzelli J, Seeholzer SH, et al. CD19 alterations emerging after CD19-directed immunotherapy cause retention of the misfolded protein in the endoplasmic reticulum. Mol Cell Biol 2018;38:e00383–18.
9. Sotillo E, Barrett DM, Black KL, Bagashev A, Oldridge D, Wu G, et al. Convergence of acquired mutations and alternative splicing of CD19 enables resistance to CART-19 immunotherapy. Cancer Discov 2015;5:1282–95.
10. Ruella M, Xu J, Barrett DM, Fraietta JA, Reich TJ, Ambrose DE, et al. Induction of resistance to chimeric antigen receptor T cell therapy by transduction of a single leukemic B cell. Nat Med 2018;24:1499–503.
11. Orlando EJ, Han X, Tribouley C, Wood PA, Leary RJ, Riester M, et al. Genetic mechanisms of target antigen loss in CAR19 therapy of acute lymphoblastic leukemia. Nat Med 2018;24:1504–6.
12. Zheng S, Asnani M, Thomas-Tikhonenko A. Escape from ALL-CAR-Taz: leukemia immunoediting in the age of chimeric antigen receptors. Cancer J 2019;25:217–22.
13. Minard-Colin V, Auperin A, Pillon M, Burke GAA, Barkauskas DA, Wheatley K, et al. Rituximab for high-risk, mature B-cell non-Hodgkin's lymphoma in children. N Engl J Med 2020;382:2207–19.
14. Sehn LH, Herrera AF, Flowers CR, Kamdar MK, McMillan A, Hertzberg M, et al. Polatuzumab vedotin in relapsed or refractory diffuse large B-cell lymphoma. J Clin Oncol 2020;38:155–65.
15. McNeer JL, Rau RE, Gupta S, Maude SL, O'Brien MM. Cutting to the front of the line: immunotherapy for childhood acute lymphoblastic leukemia. ASCO Educ Book 2020:e132–e43.
16. Ereno-Orbea J, Sicard T, Cui H, Mazhab-Jafari MT, Benlekbir S, Guarne A, et al. Molecular basis of human CD22 function and therapeutic targeting. Nat Commun 2017;8:764.
17. Nitschke L. The role of CD22 and other inhibitory co-receptors in B-cell activation. Curr Opin Immunol 2005;17:290–7.
18. Fry TJ, Shah NN, Orentas RJ, Stetler-Stevenson M, Yuan CM, Ramakrishna S, et al. CD22-targeted CAR T cells induce remission in B-ALL that is naive or resistant to CD19-targeted CAR immunotherapy. Nat Med 2018;24:20–8.
19. Brivio E, Locatelli F, Lopez-Yurda M, Malone A, Díaz-de-Heredia C, Bielorai B, et al. A phase 1 study of inotuzumab ozogamicin in pediatric relapsed/refractory acute lymphoblastic leukemia (ITCC-059 study). Blood 2021;137:1582–90.
20. O'Brien MM, Ji L, Shah NN, Rheingold SR, Bhojwani D, Yi JS, et al. A phase 2 trial of inotuzumab ozogamicin (InO) in children and young adults with relapsed or refractory (R/R) CD22+ B-acute lymphoblastic leukemia (B-ALL): results from Children's Oncology Group protocol AALL1621. Blood 2019;134:741.
21. Jain N, Maiti A, Ravandi F, Konopleva M, Daver N, Kadia T, et al. Inotuzumab ozogamicin with bosutinib for relapsed or refractory Philadelphia chromosome positive acute lymphoblastic leukemia or lymphoid blast phase of chronic myeloid leukemia. Am J Hematol 2021;96:1000–7.
22. Kantarjian HM, DeAngelo DJ, Stelljes M, Martinelli G, Liedtke M, Stock W, et al. Inotuzumab ozogamicin versus standard therapy for acute lymphoblastic leukemia. N Engl J Med 2016;375:740–53.
23. Shah NN, O'Brien MM, Yuan C, Ji L, Xu X, Rheingold SR, et al. Evaluation of CD22 modulation as a mechanism of resistance to inotuzumab ozogamicin (InO): results from central CD22 testing on the Children's Oncology Group (COG) phase II trial of INO in children and young adults with CD22+ B-acute lymphoblastic leukemia (B-ALL). J Clin Oncol 2020;38:10519.
24. Uckun FM, Goodman P, Ma H, Dibirdik I, Qazi S. CD22 EXON 12 deletion as a pathogenic mechanism of human B-precursor leukemia. Proc Natl Acad Sci U S A 2010;107:16852–7.
25. Ma H, Qazi S, Ozer Z, Gaynon P, Reaman GH, Uckun FM. CD22 exon 12 deletion is a characteristic genetic defect of therapy-refractory clones in paediatric acute lymphoblastic leukaemia. Br J Haematol 2012;156:89–98.
26. Hunger SP, Loh ML, Whitlock JA, Winick NJ, Carroll WL, Devidas M, et al. Children's Oncology Group's 2013 blueprint for research: acute lymphoblastic leukemia. Pediatr Blood Cancer 2013;60:957–63.
27. Fernandez JM, de la Torre V, Richardson D, Royo R, Puiggros M, Moncunill V, et al. The BLUEPRINT data analysis portal. Cell Syst 2016;3:491–5.
28. Vaquero-Garcia J, Barrera A, Gazzara MR, Gonzalez-Vallinas J, Lahens NF, Hogenesch JB, et al. A new view of transcriptome complexity and regulation through the lens of local splicing variations. eLife 2016;5:e11752.
29. Black KL, Naqvi AS, Asnani M, Hayer KE, Yang SY, Gillespie E, et al. Aberrant splicing in B-cell acute lymphoblastic leukemia. Nucleic Acids Res 2018;46:11357–69.
30. Soneson C, Yao Y, Bratus-Neuenschwander A, Patrignani A, Robinson MD, Hussain S. A comprehensive examination of Nanopore native RNA sequencing for characterization of complex transcriptomes. Nat Commun 2019;10:3359.

31. Hurtz C, Wertheim GB, Loftus JP, Blumenthal D, Lehman A, Li Y, et al. Oncogene-independent BCR-like signaling adaptation confers drug resistance in Ph-like ALL. J Clin Invest 2020;130:3637–53.
32. Wasim L, Buhari FHM, Yoganathan M, Sicard T, Ereno-Orbea J, Julien JP, et al. N-linked glycosylation regulates CD22 organization and function. Front Immunol 2019;10:699.
33. Psathas JN, Doonan PJ, Raman P, Freedman BD, Minn AJ, Thomas-Tikhonenko A. The Myc-miR-17-92 axis amplifies B-cell receptor signaling via inhibition of ITIM proteins: a novel lymphomagenic feed-forward loop. Blood 2013;122:4220–9.
34. Chung EY, Psathas JN, Yu D, Li Y, Weiss MJ, Thomas-Tikhonenko A. CD19 is a major B cell receptor-independent activator of MYC-driven B-lymphomagenesis. J Clin Invest 2012;122:2257–66.
35. Haso W, Lee DW, Shah NN, Stetler-Stevenson M, Yuan CM, Pastan IH, et al. Anti-CD22-chimeric antigen receptors targeting B-cell precursor acute lymphoblastic leukemia. Blood 2013;121:1165–74.
36. Handgretinger R. CAReful epitope selection matters. Blood 2013;121:1065–6.
37. Xiao X, Ho M, Zhu Z, Pastan I, Dimitrov DS. Identification and characterization of fully human anti-CD22 monoclonal antibodies. MAbs 2009;1:297–303.
38. DiJoseph JF, Popplewell A, Tickle S, Ladyman H, Lawson A, Kunz A, et al. Antibody-targeted chemotherapy of B-cell lymphoma using calicheamicin conjugated to murine or humanized antibody against CD22. Cancer Immunol Immunother 2005;54:11–24.
39. Ramakrishna S, Highfill SL, Walsh Z, Nguyen SM, Lei H, Shern JF, et al. Modulation of target antigen density improves CAR T-cell functionality and persistence. Clin Cancer Res 2019;25:5329–41.
40. Wayne AS, Shah NN, Bhojwani D, Silverman LB, Whitlock JA, Stetler-Stevenson M, et al. Phase 1 study of the anti-CD22 immunotoxin moxetumomab pasudotox for childhood acute lymphoblastic leukemia. Blood 2017;130:1620–7.
41. Kreitman RJ, Tallman MS, Robak T, Coutre S, Wilson WH, Stetler-Stevenson M, et al. Phase I trial of anti-CD22 recombinant immunotoxin moxetumomab pasudotox (CAT-8015 or HA22) in patients with hairy cell leukemia. J Clin Oncol 2012;30:1822–8.
42. Shah NN, Bhojwani D, August K, Baruchel A, Bertrand Y, Boklan J, et al. Results from an international phase 2 study of the anti-CD22 immunotoxin moxetumomab pasudotox in relapsed or refractory childhood B-lineage acute lymphoblastic leukemia. Pediatr Blood Cancer 2020;67:e28112.
43. Choi PS, Thomas-Tikhonenko A. RNA-binding proteins of COSMIC importance in cancer. J Clin Invest 2021;131:e151627.
44. Lamba JK, Chauhan L, Shin M, Loken MR, Pollard JA, Wang YC, et al. CD33 splicing polymorphism determines gemtuzumab ozogamicin response in de novo acute myeloid leukemia: report from randomized phase III Children's Oncology Group trial AAML0531. J Clin Oncol 2017;35:2674–82.
45. Tasian SK, Teachey DT, Li Y, Shen F, Harvey RC, Chen IM, et al. Potent efficacy of combined PI3K/mTOR and JAK or ABL inhibition in murine xenograft models of Ph-like acute lymphoblastic leukemia. Blood 2017;129:177–87.
46. Tasian SK, Hurtz C, Wertheim GB, Bailey NG, Lim MS, Harvey RC, et al. High incidence of Philadelphia chromosome-like acute lymphoblastic leukemia in older adults with B-ALL. Leukemia 2017;31:981–4.
47. Li H, Handsaker B, Wysoker A, Fennell T, Ruan J, Homer N, et al. The sequence alignment/map format and SAMtools. Bioinformatics 2009;25:2078–9.
48. Danecek P, McCarthy SA. BCFtools/csq: haplotype-aware variant consequences. Bioinformatics 2017;33:2037–9.